The Pex4p-Pex22p complex from Hansenula polymorpha

Ali, Ameena M; Atmaj, Jack; Adawy, Alaa; Lunev, Sergey; Van Oosterwijk, Niels; Yan, Sun Rei; Williams, Chris; Groves, Matthew R

Published in:
Acta Crystallographica Section F: Structural Biology Communications

DOI:
10.1107/S2053230X17018428

Publication date:
2018

STRUCTURAL BIOLOGY COMMUNICATIONS

ISSN 2053-230X

The Pex4p–Pex22p complex from *Hansenula polymorpha*: biophysical analysis, crystallization and X-ray diffraction characterization

Ameena M. Ali,[a] Jack Atmaj,[a] Alaa Adawy,[a] Sergey Lunev,[a] Niels Van Oosterwijk,[a] Sun Rei Yan,[a] Chris Williams[b] and Matthew R. Groves[a]*

[a]Groningen Research Institute of Pharmacy, University of Groningen, 9700 AD Groningen, The Netherlands, and [b]Molecular Cell Biology, Groningen Biomolecular Sciences and Biotechnology Institute, University of Groningen, 9700 AD Groningen, The Netherlands. *Correspondence e-mail: m.r.groves@rug.nl

Received 14 August 2017
Accepted 24 December 2017

Edited by N. Sträter, University of Leipzig, Germany

Keywords: Pex4; Pex22; ubiquitin-conjugating enzyme; peroxisome import; *Hansenula polymorpha*.

Peroxisomes are a major cellular compartment of eukaryotic cells, and are involved in a variety of metabolic functions and pathways according to species, cell type and environmental conditions. Their biogenesis relies on conserved genes known as *PEX* genes that encode peroxin proteins. Peroxisomal membrane proteins and peroxisomal matrix proteins are generated in the cytosol and are subsequently imported into the peroxisome post-translationally. Matrix proteins containing a peroxisomal targeting signal type 1 (PTS1) are recognized by the cycling receptor Pex5p and transported to the peroxisomal lumen. Pex5p docking, release of the cargo into the lumen and recycling involve a number of peroxins, but a key player is the Pex4p–Pex22p complex described in this manuscript. Pex4p from the yeast *Saccharomyces cerevisiae* is a ubiquitin-conjugating enzyme that is anchored on the cytosolic side of the peroxisomal membrane through its binding partner Pex22p, which acts as both a docking site and a co-activator of Pex4p. As Pex5p undergoes recycling and release, the Pex4p–Pex22p complex is essential for monoubiquitination at the conserved cysteine residue of Pex5p. The absence of Pex4p–Pex22p inhibits Pex5p recycling and hence PTS1 protein import. This article reports the crystallization of Pex4p and of the Pex4p–Pex22p complex from the yeast *Hansenula polymorpha*, and data collection from their crystals to 2.0 and 2.85 Å resolution, respectively. The resulting structures are likely to provide important insights to understand the molecular mechanism of the Pex4p–Pex22p complex and its role in peroxisome biogenesis.

1. Introduction

Peroxisomes are organelles that are involved in many metabolic functions and pathways, depending upon the species, cell type and environmental conditions. Such functions include the oxidation of fatty acids, the protection of cells from oxidative damage (Fujiki *et al.*, 2012; Wanders & Waterham, 2006), the metabolism of specific carbon and/or nitrogen sources, for example methanol, D-alanine, primary amines or oleic acid, in yeasts (Klei & Veenhuis, 1996), and the synthesis of plasmalogens, cholesterol and bile acids in mammals (van den Bosch *et al.*, 1992). Their biogenesis relies on highly conserved genes known as *PEX* genes that encode peroxins, which mainly function in the formation of peroxisomes or the import of matrix and membrane proteins (Fujiki *et al.*, 2012; Titorenko & Rachubinski, 2001). For example, Pex5p is a key cytosolic recycling receptor for matrix proteins imported through the peroxisomal targeting signal type 1 (PTS1) pathway (Williams & Stanley, 2010). The Pex5p import cycle can be divided into the following steps: (i) recognition of a PTS1-containing

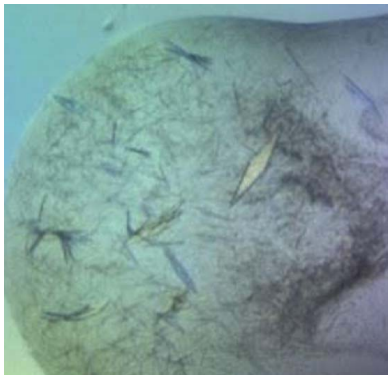

Table 1
Macromolecule-production information for Pex22^{S} and Pex4p.

Cloning details for Pex22^{S} and Pex4p from *H. polymorpha*. Restriction sites in the primers for the wild type are shown in bold. Additional residues at the N-terminus are underlined. The beginning and end numbers of the amino-acid sequences are shown as subscripts.

	Pex22^{S}	Pex4p
Source organism	*H. polymorpha*	*H. polymorpha*
DNA source	*H. polymorpha* genomic DNA	*H. polymorpha* genomic DNA
Forward primer (NcoI)	5′-**CCATGG**CCTGGGCGTTGAAGACG-3′	5′-G**CCATGG**CTTCTACAGAAAAGCGG-3′
Reverse primer (HindIII)	5′-GCG**AAGCTT**TATATATAATCATTTATACGATCC-3′	5′-GCG**AAGCTT**TATACATCATTAGATTCGTATGC-3′
Expression vector	pETM-30	pETM-30
Expression host	*E. coli*	*E. coli*
Complete amino-acid sequence of the construct produced†	GAMA$_{26}$WALKTINPGLFEEPAKTSEASKSNGQSVSLVLTQKDL DFFSAAYLNEYPNLTVILHPSVDKSEFLSRFNVQRNSHQVI QVRTEESIFHVLKQLSSNINLITLGNLEMSANEVETFHLDK FLTNVHEVDRINDYI$_{160}$	GAMAS$_{2}$TEKRLLKEYRAVKKELTEKRSPIHDTGIVDLHPLEDG LFRWSAVIRGPDQSPFEDALWKLEIDIPTNYPLDPPKIKFV VFGEEKIRQLQRKTSSGARKVCYKMPHPNVNFKTGEICLDI LQQKWSPAWTLQSALVAIVVLLANPEPLSPLNIDMANLLKC DDTTAYKDLVHYYIAKYSAYESNDV$_{188}$

† After TEV digestion.

Table 2
Crystallization of Pex4p and of the Pex4p–Pex22^{S} complex, including the final buffer compositions and the conditions in which crystals were grown.

	Pex4p	Pex4p–Pex22^{S} complex
Method	Hanging-drop vapour diffusion	Sitting-drop vapour diffusion
Plate type	24-well XRL Plate (Molecular Dimensions, catalogue No. MD11-00-100)	96-well Polystyrene MRC Crystallization Plate (Molecular Dimensions, catalogue No. MD3-11)
Temperature (K)	293	293
Protein concentration (mg ml^{-1})	12	12
Buffer composition of protein solution	25 m*M* Tris, 150 m*M* NaCl, 1% glycerol, 1 m*M* BME pH 7.5	25 m*M* Tris, 150 m*M* NaCl, 1% glycerol, 1 m*M* BME pH 7.5
Buffer composition of reservoir solution	0.1 *M* MES, 50%(*v*/*v*) PEG 200 pH 6.5	0.1 *M* bis-tris propane, 0.2 *M* sodium sulfate, 22%(*w*/*v*) PEG 3350 pH 7.8
Volume and ratio of the drops	2 µl (1:1 ratio)	320 nl (1:1 ratio)

protein by Pex5p in the cytosol (Gatto *et al.*, 2000; Stanley *et al.*, 2006), (ii) docking of the Pex5p–cargo complex at the peroxisomal membrane (Elgersma *et al.*, 1996; Albertini *et al.*, 1997), (iii) cargo translocation into the peroxisomal lumen (Meinecke *et al.*, 2010; Wang *et al.*, 2003) and (iv) recycling of Pex5p for a new import cycle (Platta *et al.*, 2007, 2008). Although the recycling of the Pex5p receptor has been studied in detail, the mechanism of cargo release remains elusive (Kim & Hettema, 2015; Girzalsky *et al.*, 2010).

The receptor-recycling step involves monoubiquitination of Pex5p at the conserved cysteine residue (Williams *et al.*, 2007; Okumoto *et al.*, 2011) and requires the action of a number of peroxins, including Pex1p, Pex4p, Pex6p, Pex15p and Pex22p (Koller *et al.*, 1999; Collins *et al.*, 2000; Platta *et al.*, 2008; Rosenkranz *et al.*, 2006). Several studies have shown that the ubiquitin-conjugating (E2) enzyme Pex4p is responsible for Pex5p monoubiquitination in the yeast *Saccharomyces cerevisiae* (El Magraoui *et al.*, 2014; Williams *et al.*, 2007; Platta *et al.*, 2007). Pex4p associates with the peroxisomal membrane *via* its interaction with the membrane-bound Pex22p (Koller *et al.*, 1999). However, Pex22p also acts as a co-activator of Pex4p, stimulating the E2 activity of Pex4p through an unknown mechanism (Williams *et al.*, 2012, 2013; El Magraoui *et al.*, 2014).

In order to understand the molecular mechanism guiding the assembly of the Pex4p–Pex22p complex, as well as the role of Pex22p as a co-activator protein, further high-resolution structural models of the partners in the complex are required. Here, we report the crystallization of Pex4p alone and in complex with the soluble domain of Pex22p (hereafter referred to as Pex22^{S}) from the yeast *Hansenula polymorpha*. Moreover, we used microscale thermophoresis to analyse the dissociation constant (K_d) of the Pex4p–Pex22^{S} complex *in vitro*.

2. Materials and methods

2.1. Cloning of Pex4p and Pex22^{S}

Escherichia coli plasmids for the expression of His$_6$-GST-tagged wild-type Pex4p and the soluble region of Pex22p (Pex22^{S}; residues 26–160) were made as follows: PCR was performed on *H. polymorpha* genomic DNA using the primer combinations HpP4 NcoI (GCCATGGCTTCTACAGAAA AGCGG) and HpP4 HindIII (GCGAAGCTTTATACAT CATTAGATTCGTATGC) for Pex4p and HpP22 NcoI (CCATGGCCTGGGCGTTGAAGACG) and HpP22 HindIII (GCGAAGCTTTATATATAATCATTTATACGATCC) for Pex22^{S}; the resulting fragments were digested with NcoI and HindIII and ligated into NcoI–HindIII-digested pETM-30 vector. For cloning details, please refer to Table 1.

2.2. Expression and purification of Pex4p and Pex22^{S}

E. coli BL21 (DE3) RIL competent cells were transformed with either the pETM-30-Pex4p or the pETM-30-Pex22^{S} expression plasmid. These plasmids encode wild-type Pex4p

and the soluble region of Pex22p, respectively, both fused to a N-terminal GST and His_6 tag. Expression of both constructs was performed according to the following protocol. The transformed colonies were selected on LB agar plates supplemented with kanamycin (25 µg ml^{-1}) and chloramphenicol (35 µg ml^{-1}). A single colony was used to inoculate a 10 ml culture of LB supplemented with kanamycin (25 µg ml^{-1}) and chloramphenicol (35 µg ml^{-1}), which was then incubated in a shaking incubator at 310 K for 4–5 h. The culture was then used to inoculate 1 l TB supplemented with kanamycin (25 µg ml^{-1}) and chloramphenicol (25 µg ml^{-1}) and allowed to grow at 310 K to an OD_{600} of 0.8. The cells were then cooled to 294 K and induced with isopropyl β-D-1-thiogalactopyranoside at a final concentration of 50 µ*M*. Both cultures were further incubated at 294 K for 18 h. After harvesting, the cell pellets were resuspended in buffer 1 [50 m*M* Tris, 300 m*M* NaCl, 1 m*M* β-mercaptoethanol (BME) pH 7.5] and lysed using a French press. The lysate was then clarified by centrifugation (18 000 rev min^{-1}; SS-34 rotor, Sorvall) before incubation with 5 ml glutathione *S*-transferase (GST) resin (GE Healthcare). The resin was further sequentially washed in buffer 1, buffer 2 (50 m*M* Tris, 1 *M* NaCl, 1% glycerol, 1 m*M* BME pH 7.5) and buffer 3 (50 m*M* Tris, 150 m*M* NaCl, 1% glycerol, 1 m*M* BME pH 7.5). The target proteins were eluted with 20–30 ml elution buffer (buffer 3 supplemented with 20 m*M* reduced glutathione). Subsequently, the eluted Pex4p and Pex22^S proteins were subjected to TEV cleavage (using a ratio of 1 mg TEV to 25 mg fusion protein) overnight at 277 K without shaking. Both TEV and the N-terminal cleavage products containing the His_6 tag were removed by passage through Ni–NTA agarose and the flowthrough was collected. Pure Pex4p and Pex22^S were present in the flowthrough, which was concentrated using centrifugal concentrators (10 000 Da molecular-weight cutoff; Vivaspin 20, Sartorius). The proteins were further purified by size-exclusion chromatography (SEC) using a Superdex 75 16/60 column (GE Healthcare) equilibrated with GF buffer (25 m*M* Tris, 150 m*M* NaCl, 1% glycerol, 1 m*M* BME pH 7.4). The Pex4p–Pex22^S complex was prepared by incubating a mixture of Pex4p and Pex22^S [at a 1:1.8 molar ratio as determined using UV spectroscopy and their tabulated extinction coefficients (https://www.expasy.org)] for 1 h on ice. The sample was further concentrated prior to injection onto an SEC column (Superdex 75 16/60; GE Healthcare) previously equilibrated with GF buffer.

2.3. Crystallization of Pex4p and the Pex4p–Pex22^S complex

Purified Pex4p was concentrated using a Vivaspin 20 concentrator (Sartorius) to 12 mg ml^{-1} for crystallization trials. Pex4p crystallization conditions were established using the high-throughput crystallization platform at the EMBL (Hamburg) and initial crystals were identified in 0.1 *M* MES, 40%(*v*/*v*) PEG 200 pH 6.5. Further optimization of the crystallization conditions resulted in high-quality crystals that were appropriate for X-ray diffraction analysis, which were obtained in 0.1 *M* MES, 50%(*v*/*v*) PEG 200 pH 6.5 from plates that were incubated at 293 K. Similarly, the Pex4p–Pex22^S complex was concentrated to 12 mg ml^{-1} and was used for crystallization trials using a Mosquito high-throughput crystallization robot (TTP Labtech). The concentration was calculated based on an assumed 1:1 complex and the respective tabulated extinction coefficients (https://www.expasy.org). Initial screening was carried out with two screening kits: PACT *premier* HT-96 and JCSG-*plus* (Molecular Dimensions). The plates were incubated at 293 K for a week and initial crystals were identified in 0.1 *M* bis-tris propane, 0.2 *M* sodium sulfate, 20%(*w*/*v*) PEG 3350 pH 7.5. After optimization of the crystallization buffer to 0.1 *M* bis-tris propane, 0.2 *M* sodium sulfate, 22%(*w*/*v*) PEG 3350 pH 7.8, a single crystal that was suitable for X-ray diffraction analysis was obtained. Table 2 summarizes the crystallization conditions. Several crystals of the complex were grown during optimization of the conditions, with fine needle shapes in a fan-like structure. These crystals were fragile and were difficult to fish out prior to diffraction studies. Seeding was not attempted.

Crystals of Pex4p as well as those of the Pex4p–Pex22^S complex were transferred to a cryobuffer consisting of the reservoir buffer supplemented with 20%(*v*/*v*) glycerol and were then flash-cooled in liquid nitrogen prior to data collection. The crystals were shipped using a dry-shipping container (Taylor–Wharton) to the PETRA III synchrotron, Hamburg, Germany for diffraction data collection.

2.4. Microscale thermophoresis (MST)

MST measurements were performed on a Nanotemper Monolith NT.115 instrument (Nanotemper Technologies GmbH). Purified Pex4p was labelled with the Monolith Protein Labelling Kit RED according to the supplied protocol (Nanotemper Technologies GmbH). The labelled protein was concentrated using a PES centrifugation filter (3 kDa cutoff; VWR), diluted with glycerol [final concentration of 50%(*v*/*v*)] and the aliquots were stored at 193 K. Measurements were performed in MST buffer (25 m*M* Tris pH 7.5, 125 m*M* NaCl, 1% glycerol, 1 m*M* BME, 0.05% Tween 20) in standard

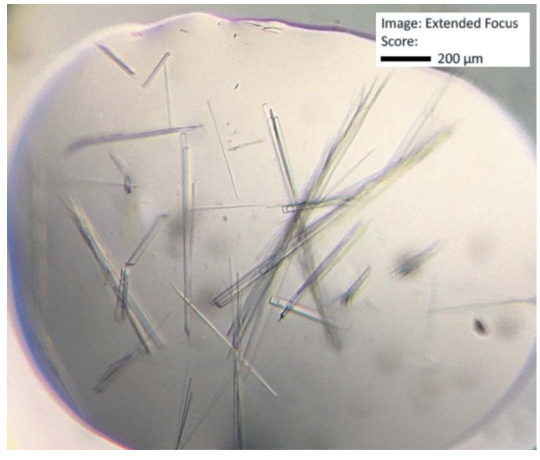

Figure 1
Needle-shaped Pex4p crystals produced in 0.1 *M* MES, 50%(*v*/*v*) PEG 200 pH 6.5.

capillaries (K002; Nanotemper Technologies GmbH). Labelled Pex4p was used at a final concentration of 10 n*M*. Pex22s was titrated in 1:1 dilutions starting at 2.82 µ*M*. All binding reactions were incubated for 10 min at room temperature followed by centrifugation at 20 000*g* before loading into capillaries. All measurements were performed in triplicate at 20% LED and 60% MST power; the laser on time was 30 s and the laser off time was 5 s.

3. Results

3.1. Crystallization of Pex4p

Full-length Pex4p protein was purified from an *E. coli*-based expression system and the purified protein was crystallized at 293 K (Fig. 1). The final crystals were grown in 0.1 *M* MES, 50%(*v*/*v*) PEG 200 pH 6.5. A single crystal was harvested in a mounted loop, directly flash-cooled in liquid nitrogen and transported to the P11 beamline at PETRA III, Hamburg for data collection and structural analysis.

3.2. Crystallization of the Pex4p–Pex22^{S} complex

An initial crystal of the Pex4p–Pex22^{S} complex was grown in a solution consisting of 0.1 *M* bis-tris propane, 0.2 *M* sodium sulfate, 20%(*w*/*v*) PEG 3350 pH 7.5 from the PACT *premier* HT-96 screening kit (Molecular Dimensions) as shown in Fig. 2(*a*). Fig. 2(*b*) illustrates the final crystal, which was grown in 0.1 *M* bis-tris propane, 0.2 *M* sodium sulfate, 22%(*w*/*v*) PEG 3350 pH 7.8. The crystal was directly harvested and flash-cooled for data collection and structural analysis as indicated above.

3.3. Data collection and processing

The Pex4p crystal used for the experiment diffracted to a resolution of 2.0 Å and X-ray data were collected on beamline P11 at the PETRA III synchrotron, DESY, Germany. The raw data were processed automatically, using the *XDS* software (Kabsch, 2010) for integration and truncation of the data. The Pex4p crystal belonged to space group $P4_12_12$, with unit-cell parameters $a = 46.35$, $b = 46.35$, $c = 206.41$ Å, $\alpha = \beta = \gamma = 90°$.

Similarly, diffraction data from the Pex4p–Pex22^{S} complex crystal were also collected on beamline P11 at the PETRA III synchrotron, DESY, Germany. The crystal diffracted to a maximal resolution of 2.85 Å. The crystal of the complex belonged to space group *P*1, with unit-cell parameters $a = 44.7$, $b = 61.6$, $c = 78.4$ Å, $\alpha = 89.2$, $\beta = 78.0$, $\gamma = 84.1°$. The raw data were processed automatically using *XDS* (Kabsch, 2010). Data-collection and processing statistics are summarized in Table 3.

Table 3
Data-collection statistics.

Values in parentheses are for the highest resolution shell.

	Pex4p	Pex4p–Pex22^{S} complex
X-ray source	PETRA III	PETRA III
Beamline	P11	P11
Wavelength (Å)	1.03	0.98
Space group	$P4_12_12$	*P*1
a, *b*, *c* (Å)	46.35, 46.35, 206.41	44.7, 61.6, 78.4
α, β, γ (°)	90, 90, 90	89.2, 78.0, 84.1
Resolution (Å)	45.22–2.00 (2.26–2.00)	76.7–2.85 (2.95–2.85)
R_{meas}†	0.147 (0.74)	0.123 (0.80)
Total No. of observations	59646 (1977)	71456 (9995)
Total No. of unique reflections	14409 (1206)	18181 (1822)
Mean $I/\sigma(I)$	6.21 (1.69)	6.03 (1.14)
Completeness (%)	92 (88)	95.02 (94.5)
Wilson *B* factor (Å^2)	42.5	48.9
Multiplicity	4.1 (1.6)	3.9 (5.48)
$CC_{1/2}$	0.995 (0.426)	0.996 (0.529)
Matthews coefficient (Å^3 Da^{-1})	2.63	2.92
Mosaicity (°)	0.13	0.42

† R_{meas} is defined as $\sum_{hkl}\{N(hkl)/[N(hkl)-1]\}^{1/2}\sum_i |I_i(hkl) - \langle I(hkl)\rangle|/\sum_{hkl}\sum_i I_i(hkl)$, where $I_i(hkl)$ is the *i*th intensity measurement of reflection *hkl* and $\langle I(hkl)\rangle$ is the average intensity from multiple observations.

(*a*) (*b*)

Figure 2
(*a*) Initial crystals grown in 0.1 *M* bis-tris propane, 0.2 *M* ammonium sulfate, 20%(*w*/*v*) PEG 3350 pH 7.5 (PACT *premier* HT-96, Molecular Dimensions). The drops were set up by the sitting-drop method with a Mosquito robot (TTP Labtech) using drops consisting of 160 nl protein solution and 160 nl precipitant solution, and the plates were incubated at 293 K. (*b*) The final crystals grown in 0.1 *M* bis-tris propane, 0.2 *M* ammonium sulfate, 22%(*w*/*v*) PEG 3350 pH 7.8. The drops were set up by the sitting-drop method with a Mosquito robot (TTP Labtech) using drops consisting of 160 nl protein solution and 160 nl precipitant solution, and the plates were incubated at 293 K.

The structure of Pex4p was solved with the *MOLREP* molecular-replacement software using the structure of *S. cerevisiae* Pex4p as a search model (PDB entry 2y9m; 31% identity and 66% similarity; Williams *et al.*, 2012); the solution had a *Z*-score of 10.0. The coordinates of the Pex4p–Pex22^{S} complex from *S. cerevisiae* (PDB entry 2y9m; 31% identity and 66% similarity for Pex4p and 15% identity and 48% similarity for Pex22^{S}) were also used as a search model to interpret the Pex4p–Pex22^{S} data from *H. polymorpha*, yielding a molecular-replacement solution (*Z*-score of 12.4) with two copies of each partner in the protein complex (Pex4p–Pex22^{S}).

3.4. Pex4p–Pex22^{S} binding

Parameters for Pex4p–Pex22^{S} complex formation were assessed using microscale thermophoresis (MST). MST relies on the motion of molecules in microscopic temperature gradients to detect minute changes in the charge, size and hydration shell of a molecule (Jerabek-Willemsen *et al.*, 2011; Wienken *et al.*, 2010). In this experiment, fluorescently labelled Pex4p, previously purified to homogeneity (see §2), was titrated with Pex22^{S}. Fig. 3 shows an MST curve for Pex4p in the presence of different concentrations of Pex22^{S}. The dissociation constant for the Pex4p–Pex22^{S} interaction was calculated to be 1.94 ± 0.39 n*M*. This is in good agreement with the reported binding affinity between Pex4p and Pex22^{S} from *S. cerevisiae* as determined by isothermal titration calorimetry (ITC): 2.00 ± 0.08 n*M* (Williams *et al.*, 2012).

4. Discussion

The structure of *H. polymorpha* Pex4p was solved by molecular replacement using the Pex4p structure from *S. cerevisiae* as a search model (PDB entry 2y9m; 31% identity and 66% similarity to *H. polymorpha* Pex4p). The structure of the *H. polymorpha* Pex4p–Pex22^{S} complex was solved using a model built from the structure of *H. polymorpha* Pex4p together with that of *S. cerevisiae* Pex22^{S} from the *S. cerevisiae* Pex4p–Pex22^{S} structure (PDB entry 2y9m; 15% identity and 48% similarity to *H. polymorpha* Pex22^{S}), yielding a clear molecular-replacement solution with two copies of *H. polymorpha* Pex4p–Pex22^{S}. Our structural analysis of *H. polymorpha* Pex4p and the Pex4p–Pex22^{S} protein complex will be reported elsewhere (manuscript in preparation).

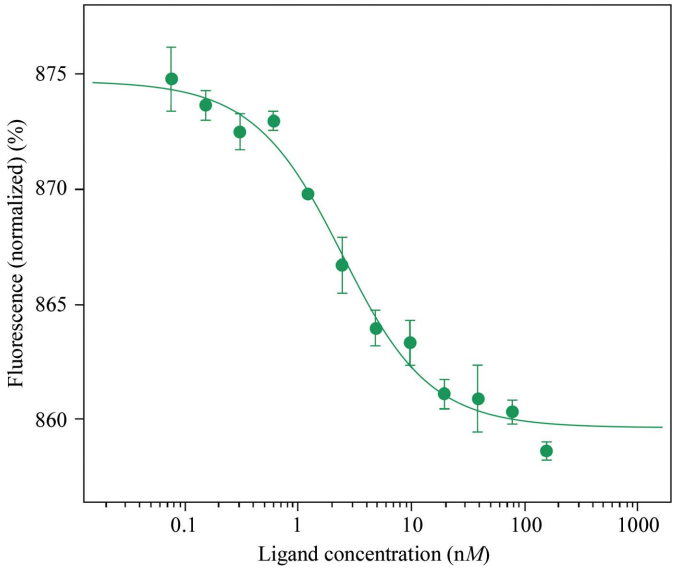

Figure 3
MST curve for the binding of Pex4p to Pex22^{S}, displaying 1:1 stoichiometry. The assay was performed using a fixed concentration of fluorescently labelled Pex4p (10 n*M*).

Pex22p acts as a co-activator of Pex4p, stimulating the activity of the E2 enzyme through an as yet unknown mechanism (Williams *et al.*, 2012, 2013; El Magraoui *et al.*, 2014). Hence, we anticipate that the structures resulting from the data reported here will provide important insights into the molecular mechanism underlying the Pex22p-dependent co-activation of Pex4p and how this impacts on the role of Pex4p in peroxisome biogenesis.

The use of MST allowed more precise insight into complex formation. The low-nanomolar dissociation constant for complex formation *in vitro* (1.94 ± 0.39 n*M*) suggests that tight binding is required for the activation of Pex4p. A 1:1 stoichiometry for the binding is also supported by our MST data (Fig. 3), as at a 1:1 ratio (10 n*M*:10 n*M*) the curve is close to saturation. Our MST data are in agreement with previous ITC data provided for the Pex4p–Pex22^{S} complex from *S. cerevisiae*, in that the dissociation constant (K_d) is equal to 2.0 ± 0.08 n*M* (Williams *et al.*, 2012). It should be borne in mind that these two affinity measurements of the Pex4p–Pex22^{S} interaction, while in good agreement, are from distinct species. As a result, a direct comparison of the methods is difficult to defend, although the MST sample requirements are significantly lower.

Acknowledgements

The authors would like to thank the staff of the P11 beamline at the PETRA III synchrotron, DESY, Hamburg for beamline access. The authors would also like to thank Dr Christian Kleusch and Dr Katarzyna Walkiewicz from Nanotemper Technologies GmbH for technical support and advice.

Funding information

CW is supported by a VIDI Grant (723.013.004) from the Netherlands Organization for Scientific Research (NWO). AMA gratefully acknowledges the Qatar Research Leadership (QRLP)–Qatar Foundation for financial support.

References

Albertini, M., Rehling, P., Erdmann, R., Girzalsky, W., Kiel, J. A., Veenhuis, M. & Kunau, W. H. (1997). *Cell*, **89**, 83–92.
Bosch, H. van den, Schutgens, R. B. H., Wanders, R. J. A. & Tager, J. M. (1992). *Annu. Rev. Biochem.* **61**, 157–197.
Collins, C. S., Kalish, J. E., Morrell, J. C., McCaffery, J. M. & Gould, S. J. (2000). *Mol. Cell. Biol.* **20**, 7516–7526.
Elgersma, Y., Kwast, L., Klein, A., Voorn-Brouwer, T., van den Berg, M., Metzig, B., America, T., Tabak, H. F. & Distel, B. (1996). *J. Cell Biol.* **135**, 97–109.

El Magraoui, F., Schrötter, A., Brinkmeier, R., Kunst, L., Mastalski, T., Müller, T., Marcus, K., Meyer, H. E., Girzalsky, W., Erdmann, R. & Platta, H. W. (2014). *PLoS One*, **9**, e105894.
Fujiki, Y., Yagita, Y. & Matsuzaki, T. (2012). *Biochim. Biophys. Acta*, **1822**, 1337–1342.
Gatto, G. J. Jr, Geisbrecht, B. V., Gould, S. J. & Berg, J. M. (2000). *Nature Struct. Biol.* **7**, 1091–1095.
Girzalsky, W., Saffian, D. & Erdmann, R. (2010). *Biochim. Biophys. Acta*, **1803**, 724–731.
Jerabek-Willemsen, M., Wienken, C. J., Braun, D., Baaske, P. & Duhr, S. (2011). *Assay Drug Dev. Technol.* **9**, 342–353.
Kabsch, W. (2010). *Acta Cryst.* D**66**, 125–132.
Kim, P. K. & Hettema, E. H. (2015). *J. Mol. Biol.* **427**, 1176–1190.
Klei, I. J. van der & Veenhuis, M. (1996). *Ann. N. Y. Acad. Sci.* **804**, 47–59.
Koller, A., Snyder, W. B., Faber, K. N., Wenzel, T. J., Rangell, L., Keller, G. A. & Subramani, S. (1999). *J. Cell Biol.* **146**, 99–112.
Meinecke, M., Cizmowski, C., Schliebs, W., Krüger, V., Beck, S., Wagner, R. & Erdmann, R. (2010). *Nature Cell Biol.* **12**, 273–277.
Okumoto, K., Misono, S., Miyata, N., Matsumoto, Y., Mukai, S. & Fujiki, Y. (2011). *Traffic*, **12**, 1067–1083.
Platta, H. W., Debelyy, M. O., El Magraoui, F. & Erdmann, R. (2008). *Biochem. Soc. Trans.* **36**, 99–104.
Platta, H. W., El Magraoui, F., Schlee, D., Grunau, S., Girzalsky, W. & Erdmann, R. (2007). *J. Cell Biol.* **177**, 197–204.
Rosenkranz, K., Birschmann, I., Grunau, S., Girzalsky, W., Kunau, W. H. & Erdmann, R. (2006). *FEBS J.* **273**, 3804–3815.
Stanley, W. A., Filipp, F. V., Kursula, P., Schüller, N., Erdmann, R., Schliebs, W., Sattler, M. & Wilmanns, M. (2006). *Mol. Cell*, **24**, 653–663.
Titorenko, V. I. & Rachubinski, R. A. (2001). *Trends Cell Biol.* **11**, 22–29.
Wanders, R. J. A. & Waterham, H. R. (2006). *Annu. Rev. Biochem.* **75**, 295–332.
Wang, D., Visser, N. V., Veenhuis, M. & van der Klei, I. J. (2003). *J. Biol. Chem.* **278**, 43340–43345.
Wienken, C. J., Baaske, P., Rothbauer, U., Braun, D. & Duhr, S. (2010). *Nature Commun.* **1**, 100.
Williams, C., van den Berg, M., Panjikar, S., Stanley, W., Distel, B. & Wilmanns, M. (2012). *EMBO J.* **31**, 391–402.
Williams, C., van den Berg, M., Sprenger, R. R. & Distel, B. (2007). *J. Biol. Chem.* **282**, 22534–22543.
Williams, C., van den Berg, M., Stanley, W. A., Wilmanns, M. & Distel, B. (2013). *Sci. Rep.* **3**, 2212.
Williams, C. P. & Stanley, W. A. (2010). *Int. J. Biochem. Cell Biol.* **42**, 1771–1774.